Title

Electrically regenerated ion-exchange technology: Leveraging faradaic reactions and assessing the effect of co-ion sorption

Authors

Gadgil, Ashok
Hackl, Lukas

Publication Date

2022-10-01

DOI

10.1016/j.jcis.2022.05.104

Peer reviewed

Electrically regenerated ion-exchange technology: Leveraging faradaic reactions and assessing the effect of co-ion sorption

Lukas Hackl[a,$,*], Shao-Wei Tsai[b,$], Bavisha Kalyan[a], Chia-Hung Hou[b,c], Ashok Gadgil[a]

[$] Denoting equal contribution

[a] *Department of Civil and Environmental Engineering, University of California Berkeley, 760 Davis Hall, Berkeley, CA 94720, USA*

[b] *Graduate Institute of Environmental Engineering, National Taiwan University, No. 1, Sec. 4. Roosevelt Rd., Taipei 10617, Taiwan*

[c] *Water Innovation, Low Carbon and Environmental Sustainability Research Center, National Taiwan University, Taipei, 10617, Taiwan*

Submitted for Publication

in

Journal of Colloid and Interface Science

February, 2022

Revised April 2022

* Corresponding Author, email: l.hackl@berkeley.edu (L. Hackl).

Abstract

Capacitive deionization (CDI) technologies have the potential to become cost-competitive alternatives to reverse osmosis for the treatment of brackish waters. In this study, we report our findings on the effect of co-ion sorption and faradaic side reactions on our ion exchange resin functionalized desalination electrodes which passively capture salt and reject it upon charging. This system, which we previously reported on and refer to as electrically regenerated ion exchange (ERI), avoids the use of expensive ion exchange membranes in an effort to save costs. Surprisingly, we find that, compared to a reference CDI system, ERI electrodes capture salt most effectively at low applied voltages (0.5 mg/cm^3 at 0.8 V). Both CDI and ERI systems also seem to suffer from co-ion sorption effects which negatively impact salt adsorption. However, Faradaic side reactions at higher voltages (1 V and 1.2 V) which we track via pH measurements, serve as a detriment to CDI but seem to facilitate the functionality of ERI.

Keywords: Capacitive deionization, Brackish groundwater desalination, Ion exchange resin, Electrically regenerative ion exchange

1. Introduction

Water security will become one of the central concerns for 21st century scientists, engineers and policy makers. To mitigate this problem, and in addition to water conservation, it is crucial to develop technologies that can produce freshwater from non-conventional sources. Groundwater with moderate salinity ranging from 1,000 ppm to 10,000 ppm, often described as "brackish" groundwater, is a promising example as it is abundant and underutilized in many arid regions of the world (e.g. the US [1] and northern India [2]). Industrially mature technologies such as reverse osmosis are not well suited to desalinate brackish groundwater, largely due the costs associated with brine disposal and membrane maintenance [3]. Electrochemical technologies such as capacitive deionization (CDI), in contrast, are capable of reducing the volume of reject brine to <10% of influent volume [4] and outcompete reverse osmosis energetically when treating brackish water sources [5]. CDI and membrane-assisted CDI (MCDI) systems capture salt ions on the surface of inexpensive, high surface area carbon electrodes and are receiving increasing scientific attention. In MCDI systems, charge-selective ion exchange membranes (IEMs) are installed in front of carbon CDI electrodes. Doing not only minimizes the occurrence of parasitic faradaic reactions that negatively impact performance [6], it also ensures that each electrode only captures ions of opposite charge (a.k.a. "counter-ions"). Without IEMs, ions of the same charge as the electrode (a.k.a. "co-ions"), can be adsorbed when the electrode potential is reversed during system regeneration or on functional groups on the carbon surface [7]. By mitigating co-ion sorption and faradaic side reactions, MCDI displays enhanced salt removal and regeneration

efficiency compared to membrane-less CDI [7]. The downside of using IEMs are added material costs that can easily increase total system costs by more than 50% [8].

Cation and anion transporting IEMs are made from sulfonated or ammoniated polystyrenes, inexpensive and widely available byproducts of petroleum refining [9]. The same polymers are also used to make cation and anion exchange resin (CER and AER) beads [10]. In the form of beads, these polymers have been used for decades in packed bed operations common in water softening [11], mining [12], chemical refining [10] and food and beverage procedures [13]. In a process called ion exchange, cations (e.g. sodium (Na^+)) and anions (e.g. chloride (Cl^-)) in the influent water will replace the protons (H^+) and hydroxide ions (OH^-) that are preloaded into the cation or anion exchange resins (CER or AER) respectively. Upon saturation with Na^+ or Cl^-, the resins are rinsed with either strong acid or base to replace cations (Na^+ with H^+) and anions (Cl^- with OH^-) to regenerate them. Comparing prices available on the websites of major resin producers such as Dow Chemicals (~0.005 $/g based on prices quoted by AlfaAesar), ion exchange beads are one to two orders of magnitudes less expensive per gram of material than ion exchange membranes. Therefore, it would be highly beneficial if the beads, rather than the membranes, could be used to build desalination electrodes.

In a previous study [14], we demonstrated proof-of-concept for an ERI system that, instead of relying on IEMs, contained powdered CER and AER beads. For construction of ERI electrodes, we mixed milled ion-exchange resin (IERs) and activated carbon (AC) in an organic solvent and cast the resulting slurry into thin-film electrodes. We found our system to behave similar to the inverted CDI systems pioneered by Gao et al. [15], capturing salt ions during 0 V operation and rejecting

them under application of an electric field. Based on simple electrochemical analysis, we've now advanced our understanding of ERI's fundamental operating principles and the system's susceptibility to co-ion sorption and faradaic side reactions. Both theses phenomena have been shown to be detrimental to CDI systems, but seem to promote the functionality of ERI [7, 16].

Specifically, we report on our results comparing ERI to CDI electrodes via cyclic voltammetry. This is followed by an analysis of the effluent pH, conductivity and overall salt adsorption capacity (SAC) of both electrode types in response to charging and discharging at different voltages. These techniques are standard practice in CDI research and have been used previously to shed light on the operating principles of various electrode-based desalination systems [5]. Surprisingly, we find that ERI electrodes capture more salt per unit electrode volume at lower applied voltages, the opposite of the trend that is observable for CDI. The effluent from the reference CDI system also undergoes wide pH fluctuations, pointing to the occurrence of acid and base producing faradaic reactions on the electrode surface. The effluent from the ERI system on the other hand is relatively pH stable. We hypothesize that the dampened effluent pH swings in the ERI system could mean that the H^+ and OH^- are in fact consumed by ion exchange reactions inside the IER particles embedded in the ERI electrodes, thereby allowing the system to be regenerated.

2. Materials and Methods

2.1 *Materials*

Anion exchange resin (AER; Amberjet® 4200, OH^- form) and cation exchange resin (CER; Amberlite® IR 120, H^+ form) were purchased from Alfa Aesar and Sigma Aldrich respectively. AC (YP-50F) was obtained from Kurrary Chemicals. N-Methyl-2-pyrrolidon (NMP, > 99%) and polyvinylidene fluoride (PVDF, MW = 534,000) were purchased from Sigma Aldrich. Food-grade 200 µm thick, polytetrafluoroethylene (PTFE) mesh was obtained from Industrial Netting. Reagent grade sodium chloride (NaCl, > 99%) was obtained from Sigma Aldrich and DI water (resistivity 18 MΩ) from a MiliQ Water pure water system by Merck.

2.2 *Electrode Fabrication*

Two types of electrodes were fabricated for this study according to the methodology of Tsai et al. [17]: electrodes made from AC only, serving as a reference system and denoted as CDI-AC electrodes from here on. And resin-functionalized ERI electrodes, denoted as ERI-CER/AER for electrodes functionalized with either cation or anion exchange resin. To make these electrodes, 5 mL of NMP were pipetted into a 20-mL vial, prepped with a stir bar, and placed on a stir plate. Under vigorous stirring, the NMP was heated to 80 °C and 0.11 g of PVDF was added in small increments, waiting for the white powder to dissolve completely and the vial contents to turn clear. The mixture was left to stir at room temperature for 0.5 h the screw-top lid closed. For the CDI-AC electrodes, 2 g of AC were slowly added to the mixture and left to stir for another 2 h. For the ERI-AER or ERI-CER electrodes, 1 g of AC and 1g of ball-milled AER or CER beads was added to the NMP-PVDF

mixture. Using a doctor blade, the resulting slurries were cast on to either titanium disks (diameter: 0.5 inch) to be used in the SwageLok electrochemical cell, or a titanium current collector (4 cm x 4 cm^2) to be used for the flow cell experiments. See Fig. S1 for a schematic of the Swagelok cell that was constructed from a Teflon T-joint to allow for parallel installation of working and counter electrodes as well as a reference electrode from the top. All electrodes were transferred to a drying oven at 80 °C overnight to completely evaporate any remaining solvent.

To confirm the embedment of IER particles in the carbon scaffold of the ERI electrodes, cross-sectional Scanning Electron Microscope (SEM) pictures were taken on a *FEI Phenom-G1*. Whereas the sulfonate functional groups on the CER beads can be distinguished well via energy dispersive X-ray (EDX) spectroscopy, the trimethyl-ammonium functional groups on AER particles are indistinguishable from the rest of the carbon scaffold. Fig. 1 therefore shows only the cross-section and accompanying EDX map of a CER-ERI electrode. In the figure, color green denotes carbon, and yellow denotes Sulphur, the latter element being unique to the CER's sulfonate functional groups. Fig. 1(b) clearly shows the presence of sulfonated CER particles throughout the electrode, with larger resin particles having settled close to current collector at the bottom of the picture. Smaller resin particles in contrast seem more uniformly dispersed throughout the carbon scaffold. We used EDX mapping solely to draw qualitative conclusions about the morphology, not to calculate sulfate density or exact location.

2.3 *Thin-film thickness and conductivity measurements*

The thickness of all dried electrodes was measured using an electronic micrometer and averaged over 2 measurements (center and edge) for the SwageLok electrodes and 5 measurements (4 corners and center) for the flow cell sized electrodes. The thin film resistance of each electrode was determined with an *Ossila* four-point probe setup and converted into a thin film conductivity by normalizing the resistance value by the electrode thickness.

2.4 *Electrochemical characterization*

For these measurements, a Swagelok cell was filled with 5 mL of nitrogen-sparged 1 M NaCl and connected to a potentiostat (Interface 1000, Gamry) as shown in Fig. S1. Two layers of carbon cloth were used as the counter electrode separated from the working electrode using a nanoporous Celgart spacer. The cyclic Voltammetry (CV) measurements were conducted by sweeping at various scan rates between 0.8 V and 0 V, −0.5 V or −0.8 V vs. Ag/AgCl. The specific capacitance (F/g) of electrode material was calculated based on Eq. (1) [18]:

$$C\ (\mathrm{F/g}) = \frac{\int_{V_a}^{V_c} I dV}{2mv(V_c - V_a)} \qquad \text{Eq. (1)}$$

where C is specific capacitance (F/g), V_c and V_a are the cutoff values of the voltage window (V), I is the response current (A), m is the mass of the IER-functionalized working electrode (g), and v is the potential scan rate (V/s). The electrochemical impedance spectroscopy (EIS) was performed at 5 mV voltage amplitude in a frequency range from 0.01 to 100000 Hz.

178

179 2.5 *Flow cell pH and conductivity measurements*

180 The CDI/ERI flow cell consisted of two parallel electrodes separated by a 1
181 mm-thick non-conductive mesh spacer. To serve as a reference CDI system, 2
182 identical CDI-AC electrodes were operated in parallel. To model an ERI system, ERI-
183 AER electrode (as the cathode) was operated in parallel with an ERI-CER electrode
184 (as the anode). Before data collection, each set of electrodes was conditioned for 10
185 charge-discharge cycles. The experimental setup for the CDI/ERI flow experiments
186 comprised a peristaltic Mettler Toledo pump, a potentiostat (Interface 1000,
187 GAMRY) and a conductivity/pH multimeter (ORION VERSASTAR, Thermo
188 scientific) as shown in Fig. S2. The flow cell was operated in single-pass mode by
189 continuously pumping 500 mg/L NaCl solution through the cell at a flow rate of 9
190 mL/min. Note that the salt capture of ERI is achieved by passive adsorption of the
191 IER-functionalized electrodes, a longer discharging time for salt capture is required
192 than the charging time for regeneration of electrodes under applied voltage. The cell
193 was charged at 0.8 V, 1.0 V or 1.2 V for 8 minutes and then operated at 0 V for 22
194 minutes by using the potentiostat. Changes in effluent conductivity and pH were
195 monitored via the conductivity/pH multimeter. Note that the working volume of the
196 IER only accounted for approximate 16% in the ERI-CER/AER electrode due to its
197 higher density (1.8 g/cm^3) than AC's density (0.37 g/cm^3) [14]. We defined the AC
198 and IER were electrode substrate and decoration for ERI electrode, respectively, on
199 the basis of working volume of the electrode. To compare the salt capture
200 performance of CDI and ERI electrode more reasonably, the volumetric salt
201 adsorption capacity (SAC) was calculated according to Eq. (2) [18]:

$$SAC(\mathrm{mg/cm^3}) = \frac{\varphi \int_0^t (C_i - C_t)dt}{v_{vol}} \quad \text{Eq. (2)}$$

Here, C_i and C_t are the initial concentration and concentration (mM) at time t (min), respectively, φ is the water flow rate (L/min) and v_{vol} (cm^3) is the volume of CDI or ERI electrode material. The concentration of NaCl solution was derived from the effluent conductivity, based on a calibration curve corresponding to each salt concentration.

3. Results and Discussion

3.1 *Faradaic reactions in Swagelok cell CDI and ERI systems*

CDI-AC, ERI-CER and ERI-AER electrodes were characterized electrochemically via CV analysis. These measurements were carried out in a Swagelok cell, with applied voltages swept between 0.8 V and –0.2 V, –0.5 V or –0.8 V vs. Ag/AgCl, at various scan rates. The resulting currents were converted into specific capacitance (F/g) values for each electrode as outlined in the methods section. Fig.2(a)–(c) shows the results of scans swept from -0.8 V to 0.8 V vs. Ag/AgCl for all three types of electrodes. The remaining CV results are show in Fig.S4–S6.

What can clearly be discerned in Fig. 2(a) is the appearance of faradaic current spikes at around +0.8V and – 0.8V in the case of CDI-AC electrodes, especially at lower scan rates. These peaks are absent from the narrower voltage window scans which are shown in Fig. S4–S6 (a)–(b). Thus, CDI-AC electrodes display purely

capacitive behavior only over relatively smaller voltage rages. A variety of proton consuming and proton generating faradaic reactions have previously been reported to occur on the surface of AC at higher voltages [19] and explain the appearance of these peaks. Of specific importance are the following half-cell reactions (namely: carbon oxidation (1) on the anode and oxygen (2) and carbon (3) reduction on the cathode), which have all have been shown to occur at potentials well within the usual CDI operating window of 1.2 V [20]:

(1) $C + H_2O \rightarrow C-OH + H^+ + e^-$

(2) $O_2 + 2H^+ + 2e^- \rightarrow H_2O_2$

(3) $C + H_2O + e^- \rightarrow C-H + OH^-$

In the context of CDI and desalination, these faradaic side-reactions are considered parasitic as they divert energy away from non-faradaic charge storage, decrease coulombic desalination efficiency, degrade the electrode and affect effluent pH [19]. For ERI, on the other hand, localized acid and base production is very much desirable to drive the exchange of Na^+ and Cl^- with H^+ and OH^- respectively during system regeneration. Both CER- (Fig. 2(b)) and AER-functionalized (Fig. 2(c)) ERI electrodes also display clear faradaic peaks at 2 mV/s scan rate. The peaks appear in the same location as for CDI-AC CV scans, that is at −0.8 V and ~0.7 V.

Ranging between ~ −40–60 F/g, ERI electrodes display comparatively lower specific capacitances than CDI-AC electrodes however which range between −150–100 F/g. A possible explanation for this is the fact that ERI electrodes, due to their functionalization with non-conducting IER particles, display film conductivities about 50% lower than those of CDI-AC electrodes (see Fig. S7). A lower film conductivity means a higher overpotential barrier for non-faradaic charge storage and for faradaic

charge transfer reactions. Furthermore, the Nyquist plot of EIS measurement showed that the ERI-electrode had significantly higher charge transfer resistances (the size of semi-circle) than the CDI-AC electrode, as shown in Fig. S8.

The effect of faradaic side reactions on effective salt adsorption capacity (SAC) is difficult to discern from CV measurements. Therefore, the following flow cell experiments were performed on larger sets (4 x 4 cm^2) of ERI and CDI electrodes. While experimental specifics are outlined in the methods section, it is important to point out that the flow cell experiments were carried out at applied voltages beyond 0.8V to ensure faradaic reactions to be taking place. Continuous pH measurements served as a proxy to track the occurrence of these faradaic reactions, whereas effluent conductivity was tracked to determine the electrodes' SAC. In this flow cell, and due to the absence of a refence electrode, the operating voltages were applied between cathode and anode.

3.2 *Faradaic reactions and co-ion sorption during flow cell experiments*

Fig. 3 shows the change in effluent conductivity and effluent pH collected for sets of pre-conditioned CDI-AC and ERI-CER/AER electrodes. For ERI, the CER containing electrode is always operated as the anode, and the AER containing electrode is always operated as the cathode. CDI and ERI electrode pairs were subjected to continuous charge-discharge cycles, charging occurring at various voltages held for 8 minutes and discharging occurring at 0 V held for 22 minutes. Asymmetry between cycles is required because charge capture in the resins (ERI) is a slow, diffusion-driven process, whereas charge capture on carbon (CDI) is an electromigration process and occurs relatively faster. Though longer than necessary,

the 0 V period was kept at 22 minutes to allow the system to return to equilibrium and be flushed of all faradaically produced species. Several interesting features can be observed from the CDI and ERI effluent parameters, as shown in Fig. 3.

For CDI (Fig. 3(a), (c)), the effluent conductivity increases above baseline (i.e., influent conductivity) for the first 2 minutes of charging and drops below baseline for the remainder of the charge cycle until minute 8. During the discharge cycle, salt desorbs from the electrodes and results in a positive spike in effluent conductivity. It is worth noting that some salt co-ions are first expelled from the carbon electrodes before more salt is captured, precisely the phenomenon of co-ion expulsion [7]. As is to be expected, co-ion sorption becomes more pronounced as the applied voltage is increased from 0.8 V to 1.2 V. The increasing prevalence of co-ion expulsion reduced the desalination performance of CDI in the beginning of the charge cycle.

Besides of co-ion expulsion, an increase in applied voltage is also associated with wider swings in effluent pH (Fig. 3(c)). While pH remains between 5.2 and 8.5 at 0.8 V operation, it drops as low as 4.5 goes as high as 9 for 1.2 V operation. This suggests that the faradaic reactions which produce H^+ and OH^- are occurring at higher rates as operating voltages increase; this is accordance with the findings reported in other studies [21]. The volumetric SAC for CDI (i.e. the integral of the effluent conductivity from 0–8 minutes shown in Fig. 4) increases by ~33% when the applied voltage is increased from 0.8 V to 1.0 V, but by less than 2% when increased to 1.2 V. Herein, the amount of salt desorption at 1.2 V was higher than that at 1.0 V, as shown in Fig. S9, suggesting that the strong generation of H^+ at 1.2 V may interfere the effluent conductivity measurement and lead to an underestimated SAC.

For ERI (Fig. 3(b), (d)), the functional groups of IER in the ERI electrodes can capture ions from water by ion exchange of H^+ or OH^- during the discharge cycle. During the charge cycle (0–8 min), effluent conductivity spikes drastically, indicating that ions are forced out of the IER-functionalized electrodes. This repulsion peak can be explained by the simple dynamic model of inverted CDI, which described the co-ions repulsed from the micropores with immobile chemical charges by applying external voltage [22]. In the beginning of the discharge cycle, some smaller spikes were followed by the regeneration peaks. This second set of peaks suggests that co-ions were adsorbed to the AC portion of the ERI electrodes during the charging operation (1.0 V and 1.2 V) and desorb during 0 V operation. The co-ion repulsion at ~9 minutes, also plays a role for ERI, and is most pronounced for 1.2 V and least pronounced for 0.8 V. Beyond 10 minutes of the discharge cycle, effluent conductivity drops below baseline suggesting that salt is being captured passively by the IER particles on the respective ERI electrode. Contrary to CDI, however, as shown in Fig. 4, volumetric salt capture in ERI (i.e. the integral of the effluent conductivity from 8–22 minutes) is highest at 0.8 V, on par with the volumetric SAC of the CDI system at 1.0 V.

This surprising outcome is illuminated by the pH data shown in Fig. 3(d). Irrespective of applied voltage, effluent pH for the ERI fluctuates only between 5 and 6, far less than the 4.5-point swing observed in the CDI case. The lower film conductivities and higher charge transfer resistances of ERI-CER/AER electrodes certainly explain part of this phenomenon. We would also like to suggest that most of the locally produced H^+ and OH^- is in fact contributing to the regeneration of the ERI electrodes. Instead of being transported out of the flow cell, H^+ and OH^- were likely

to exchange with Na^+ and Cl^- on the functional groups of CER and AER, respectively, during the charge cycle. Consequently, the large effluent spikes of conductivity (represented Na^+ and Cl^-) and mild pH fluctuation were observed during that time. Furthermore, ERI had a balanced salt adsorption and desorption at varied voltages, as shown in Fig.4 and Fig. S9. The fact that the ERI system has been shown to operate reliably for several days and without external input of acid or base [14], necessitates that these species be produced in-situ and this could be the mechanism to explain the pH response in ERI.

To confirm the cycling stability of ERI and CDI, the effluent conductivity and pH profiles over consecutive charge-discharge cycles of both systems at 0.8 V were compared, as shown in Fig. 5. ERI exhibited a promising cycling stability than CDI in terms of less desalination performance decay (Fig. 5(a)) and smaller pH fluctuations (Fig. 5(b)). In our case in CDI, the strong pH swing arisen from faradaic side reactions persistently occurred in every cycle on the CDI-AC electrode, which might cause electrode degradation, resulting in declined desalination performance [23]. These results again indicated that the IER embedded in the ERI electrode can consume the produced H^+ and OH^- from faradaic side-reactions on AC and is beneficial to maintain a stable desalination performance of the system.

4. Conclusions

The electrically regenerated ion-exchange (ERI) system was developed to serve as a low-cost alternative to other capacitive brackish water desalination systems such as CDI or MCDI. ERI employed inexpensive IER powders with the conductive AC electrode to passively capture salt and reject it upon charging. Unlike the reference

CDI system, ERI performs best at the lowest applied voltage we explored, of 0.8 V. This is because, compared to AC, IERs (which serve as the functional ingredient in ERI electrodes) have a much higher volumetric salt adsorption capacity. Moreover, two phenomena limit the performance of CDI systems: co-ion sorption and the occurrence of faradaic side reactions. Our results showed that co-ion sorption clearly diminished the salt adsorption performance of CDI and ERI electrodes alike. On the other hand, the faradaic side reactions, as tracked by effluent pH changes, were detrimental to CDI performance while which allowed the ERI system to be functional in the first place. We proposed that ERI leverages the faradaic side reactions and utilizes produced H^+ and OH^- to regenerate the IER particles incorporated in the electrodes. Faradaic side reactions drive the functionality of the ERI system, whereas they oppose the functionality of CDI systems. While more work is needed to decouple faradaic from non-faradaic processes and understand the operation principles behind the ERI system at higher resolution, ERI offers a promising approach to using of conventional and inexpensive water treatment materials for desalination of brackish water sources.

Acknowledgements

We acknowledge that support for this research was provided by the U.S. Department of Energy (DOE) U.S.-China Clean-Energy Research Center - Water Energy Technologies (Grant No. DE-IA0000018) and by the Development Impact Lab, with support from the USAID Global Development Lab and Higher Education Solutions Network (Cooperative Agreement AID-OAA-A-13-00002), hosted at the Blum Center for Developing Economies at UC Berkeley. Work at the Molecular Foundry was supported by the Office of Basic Energy Sciences of the U.S.

Department of Energy under Contract No. DEAC02-05CH11231. Shao-Wei Tsai acknowledges support from the Ministry of Science and Technology, Taiwan (109-2223-E-002-002-MY3; 106WMRFA0100033).

References

[1] J.S. Stanton, D.W. Anning, C.J. Brown, R.B. Moore, V.L. McGuire, S.L. Qi, A.C. Harris, K.F. Dennehy, P.B. McMahon, J.R. Degnan, J.K. Böhlke, Brackish groundwater in the United States, 2017. https://doi.org/10.3133/pp1833.

[2] F. Van Weert, Global Overview of Saline Groundwater Occurrence and Genesis, 2009.

[3] V.B. Jensen, J.L. Darby, Brine Disposal Options for Small Systems in California's Central Valley, *J. Am. Water Works Assoc.* 108 (2016) E276–E289. https://doi.org/10.5942/jawwa.2016.108.0045.

[4] A. Ramachandran, D.I. Oyarzun, S.A. Hawks, M. Stadermann, J.G. Santiago, High water recovery and improved thermodynamic efficiency for capacitive deionization using variable flowrate operation, *Water Res.* 155 (2019) 76–85. https://doi.org/10.1016/j.watres.2019.02.007.

[5] Y. Oren, Capacitive deionization (CDI) for desalination and water treatment - past, present and future (a review), *Desalination.* 228 (2008) 10–29. https://doi.org/10.1016/j.desal.2007.08.005.

[6] W. Tang, D. He, C. Zhang, P. Kovalsky, T.D. Waite, Comparison of Faradaic reactions in capacitive deionization (CDI) and membrane capacitive deionization (MCDI) water treatment processes, *Water Res.* 120 (2017) 229–237. https://doi.org/10.1016/j.watres.2017.05.009.

[7] H. Li, L. Zou, Ion-exchange membrane capacitive deionization: A new strategy

for brackish water desalination, *Desalination*. 275 (2011) 62–66. https://doi.org/10.1016/j.desal.2011.02.027.

[8] S. Hand, J.S. Guest, R.D. Cusick, Technoeconomic Analysis of Brackish Water Capacitive Deionization: Navigating Tradeoffs between Performance, Lifetime, and Material Costs, *Environ. Sci. Technol.* 53 (2019) 13353–13363. https://doi.org/10.1021/acs.est.9b04347.

[9] T. Luo, S. Abdu, M. Wessling, Selectivity of ion exchange membranes: A review, *J. Memb. Sci.* 555 (2018) 429–454. https://doi.org/10.1016/j.memsci.2018.03.051.

[10] F.G. Helfferich, Ion exchange, Dover Publications, 1995.

[11] A. Tabatabai, J.F. Scamehorn, S.D. Christian, Economic feasibility study of polyelectrolyte-enhanced ultrafiltration (PEUF) for water softening, *J. Memb. Sci.* 100 (1995) 193–207. https://doi.org/10.1016/0376-7388(94)00220-S.

[12] V.J. Inglezakis, M.D. Loizidou, H.P. Grigoropoulou, Ion exchange of Pb^{2+}, Cu^{2+}, Fe^{3+}, and Cr^{3+} on natural clinoptilolite: Selectivity determination and influence of acidity on metal uptake, *J. Colloid Interface Sci.* 261 (2003) 49–54. https://doi.org/10.1016/S0021-9797(02)00244-8.

[13] J. Kammerer, R. Carle, D.R. Kammerer, Adsorption and ion exchange: Basic principles and their application in food processing, *J. Agric. Food Chem.* 59 (2011) 22–42. https://doi.org/10.1021/jf1032203.

[14] C. V. Subban, A.J. Gadgil, Electrically regenerated ion-exchange technology for desalination of low-salinity water sources, Desalination. 465 (2019) 38–43. https://doi.org/10.1016/j.desal.2019.04.019.

[15] X. Gao, A. Omosebi, J. Landon, K. Liu, Surface charge enhanced carbon

electrodes for stable and efficient capacitive deionization using inverted adsorption–desorption behavior, *Energy Environ. Sci.* 8 (2015) 897–909. https://doi.org/10.1039/C4EE03172E.

[16] C. Zhang, D. He, J. Ma, W. Tang, T.D. Waite, Faradaic reactions in capacitive deionization (CDI) - problems and possibilities: A review, *Water Res.* 128 (2018) 314–330. https://doi.org/10.1016/J.WATRES.2017.10.024.

[17] S.W. Tsai, A. Kumar, B. Kalyan, C.H. Hou, P.C. Chiang, A.J. Gadgil, Additive manufacturing of electrodes for desalination, in: *Procedia Manuf.*, Elsevier B.V., 2019: pp. 252–259. https://doi.org/10.1016/j.promfg.2019.06.147.

[18] Electrochemical Systems, 3rd Edition | Wiley, (n.d.). https://www.wiley.com/en-us/Electrochemical+Systems%2C+3rd+Edition-p-9780471477563 (accessed January 21, 2021).

[19] W. Tang, D. He, C. Zhang, P. Kovalsky, T.D. Waite, Comparison of Faradaic reactions in capacitive deionization (CDI) and membrane capacitive deionization (MCDI) water treatment processes, *Water Res.* 120 (2017). https://doi.org/10.1016/j.watres.2017.05.009.

[20] T. Kim, J. Yu, C. Kim, J. Yoon, Hydrogen peroxide generation in flow-mode capacitive deionization, *J. Electroanal. Chem.* 776 (2016) 101–104. https://doi.org/10.1016/j.jelechem.2016.07.001.

[21] S. Hand, J.S. Guest, R.D. Cusick, Technoeconomic Analysis of Brackish Water Capacitive Deionization: Navigating Tradeoffs between Performance, Lifetime, and Material Costs, *Environ. Sci. Technol.* 53 (2019) 13353–13363. https://doi.org/10.1021/acs.est.9b04347.

[22] P.M. Biesheuvel, H.V.M. Hamelers, M.E. Suss, Theory of Water Desalination by

Porous Electrodes with Immobile Chemical Charge, *Colloids Interface Sci. Commun*. 9 (2015), 1-5. https://doi.org/10.1016/j.colcom.2015.12.001.

[23] He, D., Wong, C.E., Tang, W.W., Kovalsky, P. and Waite, T.D. Faradaic Reactions in Water Desalination by Batch-Mode Capacitive Deionization. Environ Sci Tech Let 3(5) (2016), 222-226. https://doi.org/10.1021/acs.estlett.6b00124

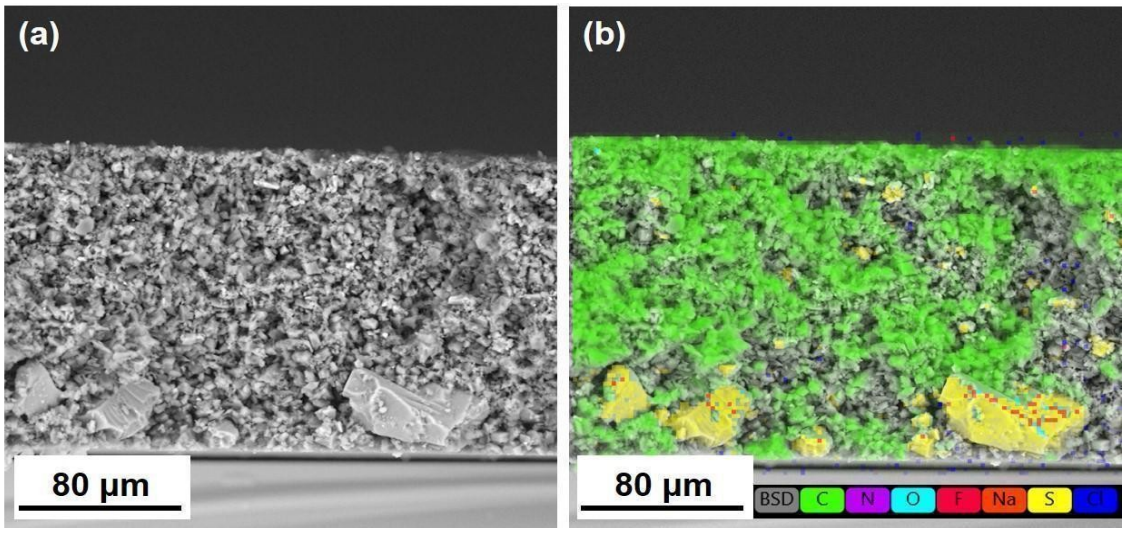

Fig. 1. Cross-sectional SEM micrographs of ERI-CER electrode without (a) and with (b) EDX mapping. EDX map in (b) clearly depicts the presence of SO_3^- (yellow) containing CER particles embedded within the AC matrix (green).

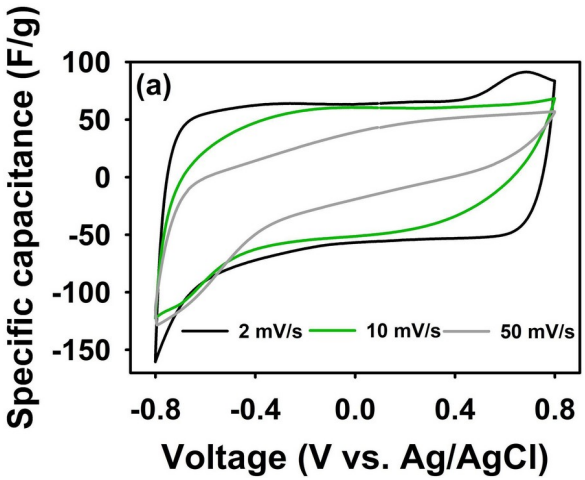

455

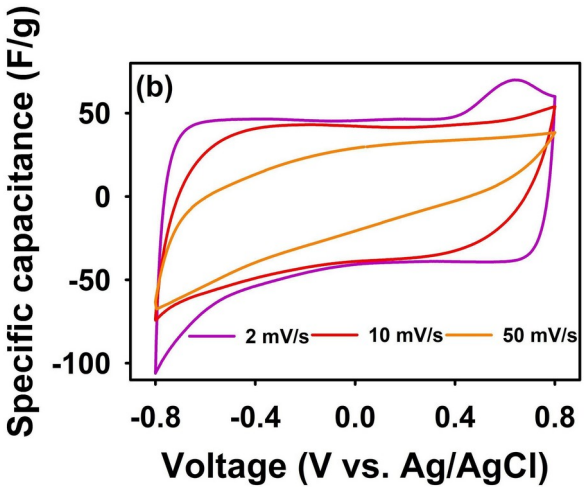

456

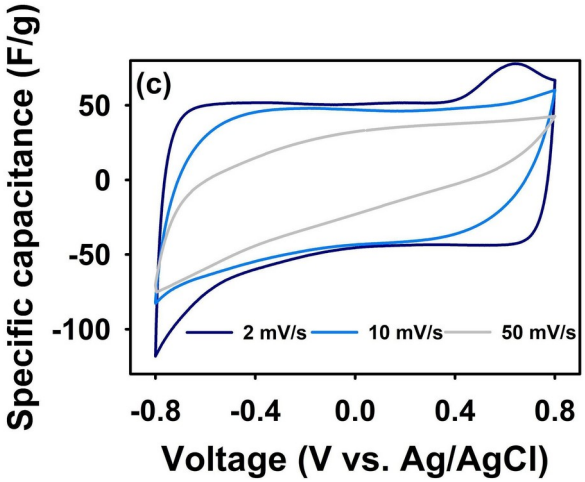

457

458 **Fig. 2.** Cyclic Voltammetry plots for (a) CDI-AC electrode (b) ERI-CER electrode

459 and (c) ERI-AER electrode scanned at 2, 10 and 50 mV/s.

460

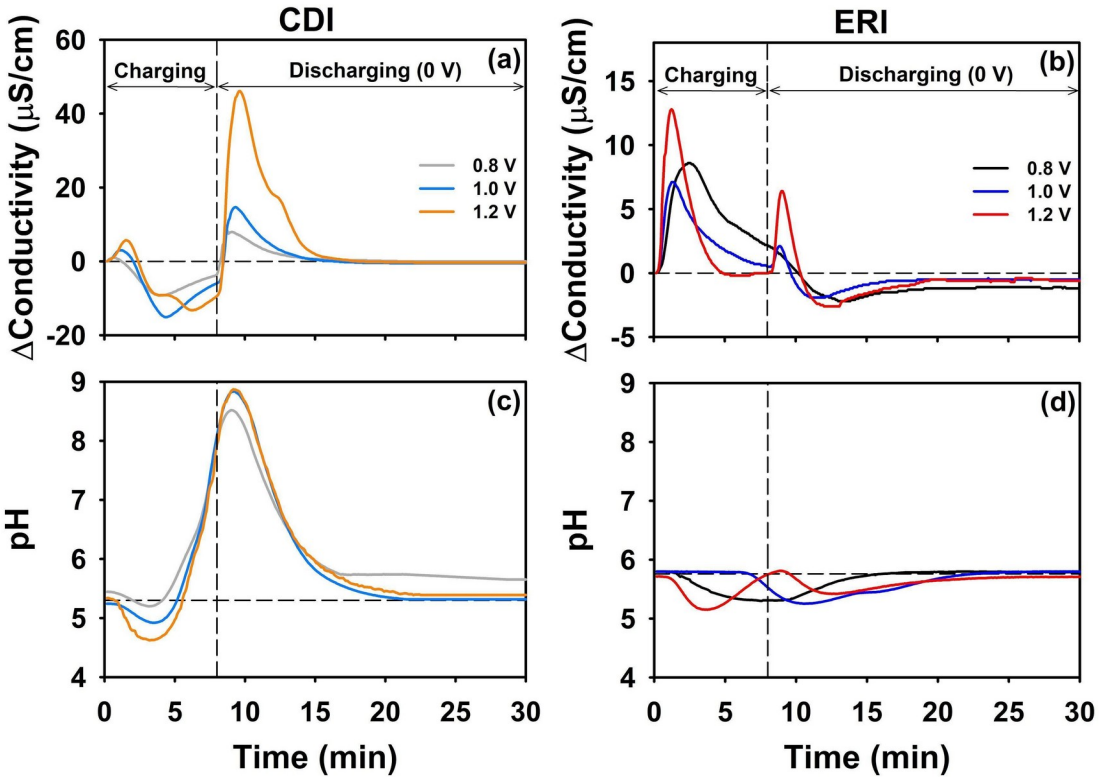

461

462 **Fig. 3.** Effluent conductivity and pH signal for 12th charge-discharge cycle. Panel (a)

463 and (b) are for CDI-AC electrodes, panel (c) and (d) for ERI-AER/CER electrodes.

464

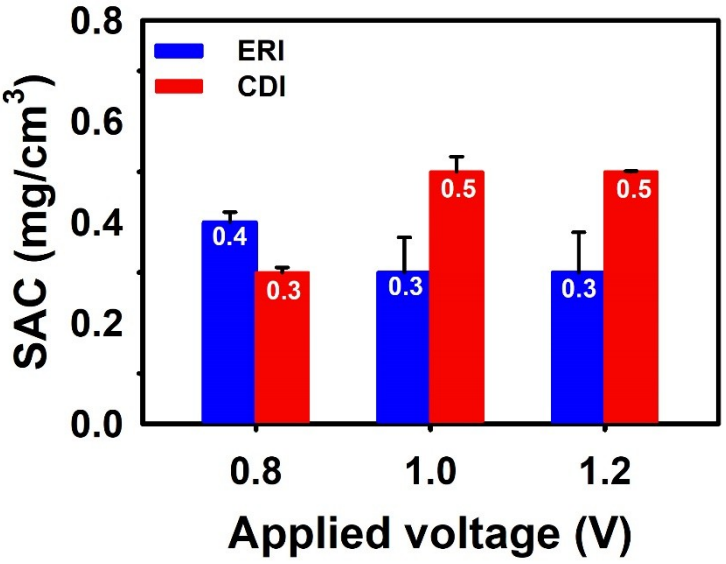

Fig. 4. Volumetric salt adsorption capacity (in mg NaCl per cm^3 electrode volume) for ERI and AC-CDI systems at different applied voltages. The error bars represented the standard deviations (SDs) on the basis of independent three charge-discharge cycles.

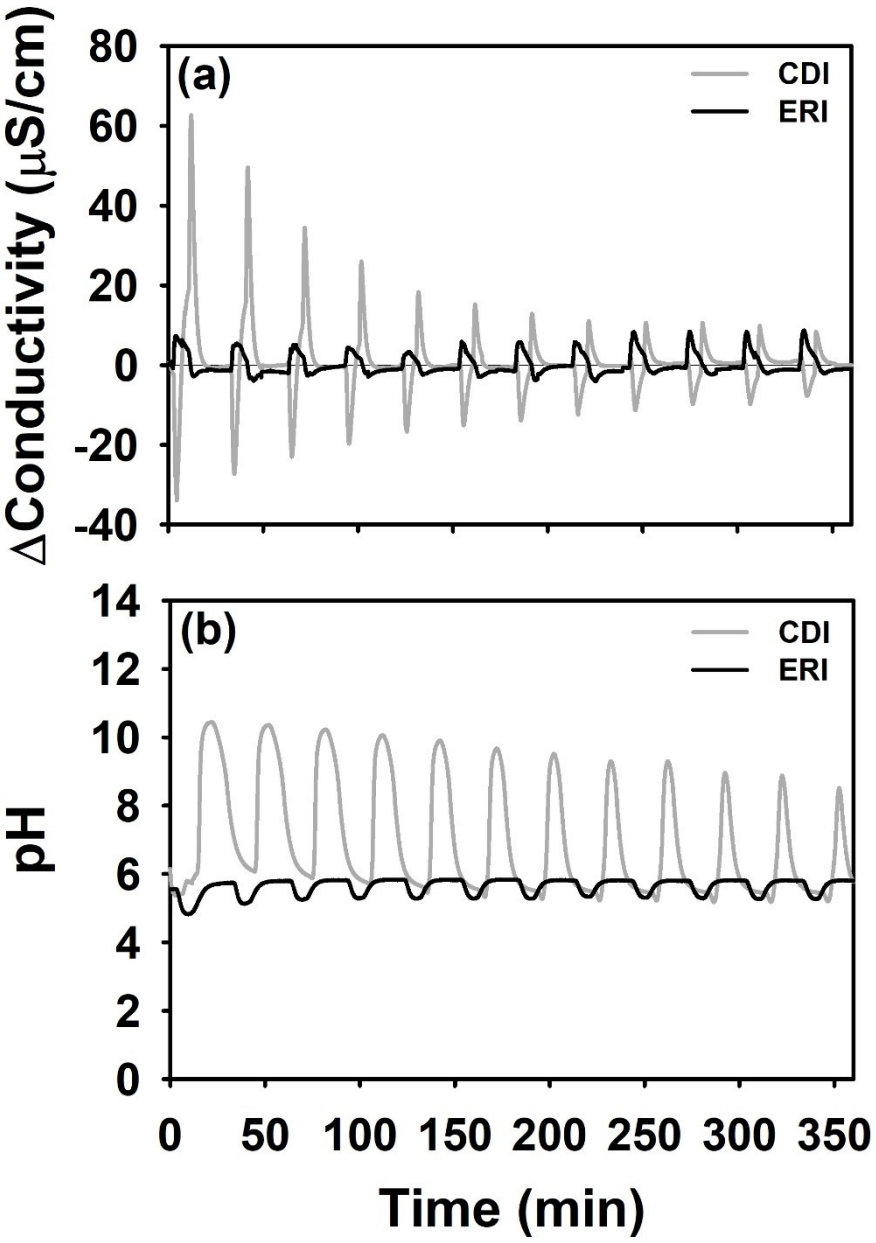

Fig. 5. (a) Effluent conductivity and (b) pH curves of CDI and ERI operation over consecutive charge/discharge cycles at 0.8 V/ 0V.